Supporting Information

Revealing Weak Dimensional Confinement Effects in Excitonic Silver/Bismuth Double Perovskites

Martina Pantaler[1,2±], Valentin Diez-Cabanes[3,4±], Valentin I. E. Queloz[2], Albertus Sutanto[2], Pascal Alexander Schouwink[5], Mariachiara Pastore[4], Inés García-Benito[2], Mohammad Khaja Nazeeruddin[2], David Beljonne[3], Doru C. Lupascu[2], Claudio Quarti[3,*] and Giulia Grancini[6,*]

[1] Institute for Materials Science and Center for Nanointegration Duisburg-Essen (CENIDE), University of Duisburg-Essen, Universitätsstraße 15, 45141 Essen

[2] Group for Molecular Engineering of Functional Materials, Institute of Chemical Sciences and Engineering, Ecole Polytechnique Fédérale de Lausanne, Sion CH-1951, Switzerland.

[3] Laboratory for Chemistry of Novel Materials, University of Mons, Place du Parc 20, B-7000 Mons, Belgium

[4] Université de Lorraine & CNRS, LPCT, UMR 7019, F-54000 Nancy, France

[5] Institute of Chemical Sciences and Engineering, Ecole Polytechnique Fédérale de Lausanne (EPFL) CH-1015 Lausanne, Switzerland

[6] Department of Chemistry & INSTM, University of Pavia, Via Torquato Taramelli 14, Pavia 27100, Italy

[±] These authors equally contributed to the paper.

*corresponding author: giulia.grancini@unipv.it, claudio.quarti@umons.ac.be

Crystal structure and morphologic characterization of PeABr1 and PeABr2 thin films

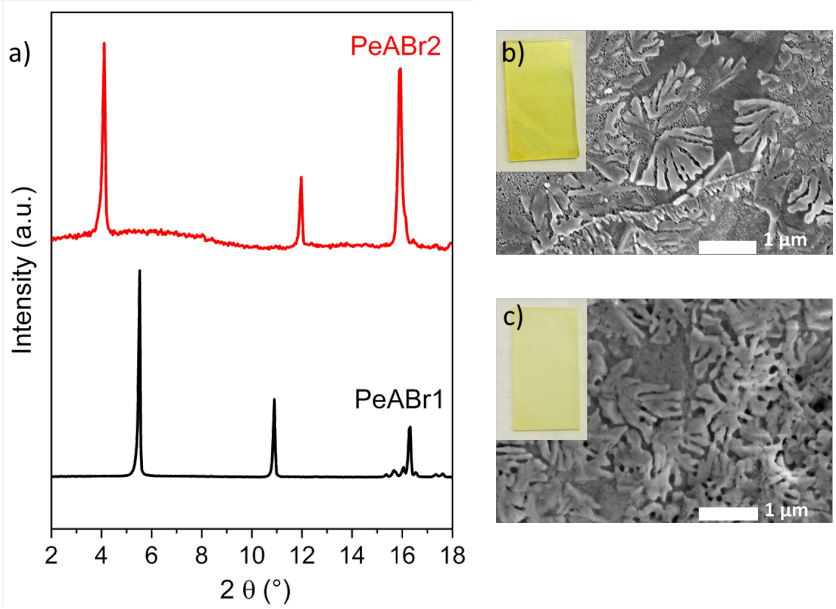

Figure S1. a) XRD patterns of thin films for PeABr2 and PeABr1 **b)** SEM image of PeABr2 and **c)** SEM image of PeABr1

Descriptors for the structural deformations from the ideal perovskite structure

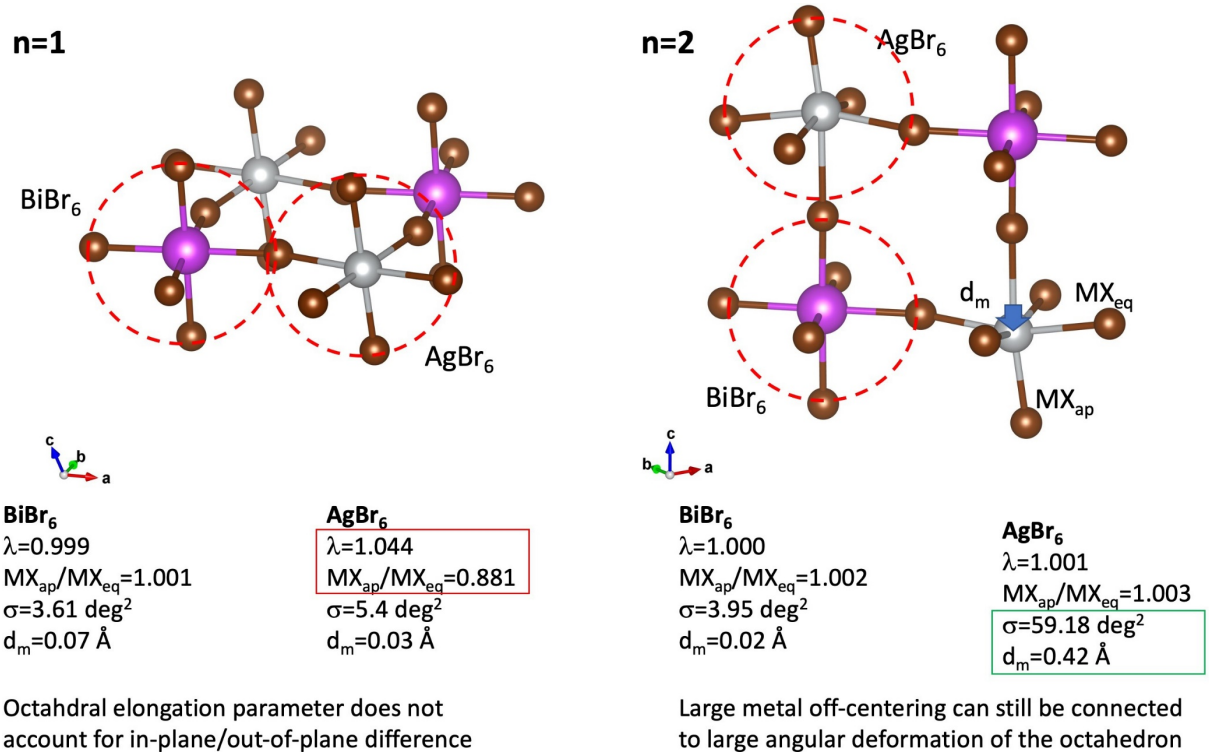

Figure S2. Structural descriptors for Jahn-Teller distortions and metal off-centering in *n*=1 (left panel) and *n*=2 (right panel) layered 2D double halide perovskites; λ and σ correspond to widely reported octahedral elongation and octahedral distortion parameters, respectively. MX_{ap} and MX_{eq} correspond to metal-to-apical halide and metal-to-equatorial halide distance, respectively; d_m corresponds to the metal off-centering with respect to the plane of the equatorial halides.

First Brillouin zones for the investigated compounds and correspondence between indirect space high symmetry points and real space directions

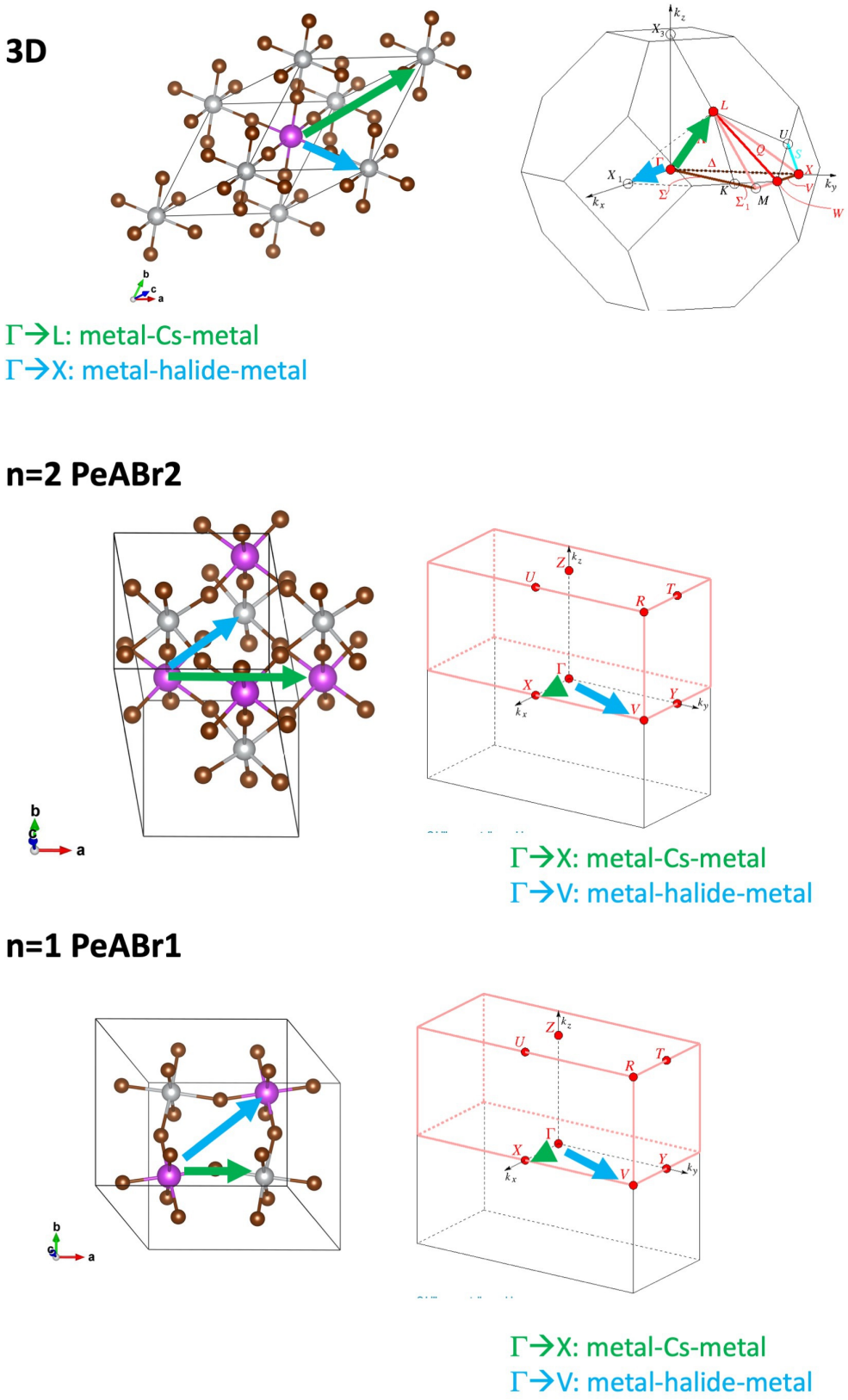

Figure S3. Correspondence between high symmetry directions in the direct lattices with Fm-3m and P-1 symmetry and high symmetry points in their corresponding Brillouin zones.

Band folding for n=1 layered double perovskite: band structure from XRD crystallographic model and from reduced model

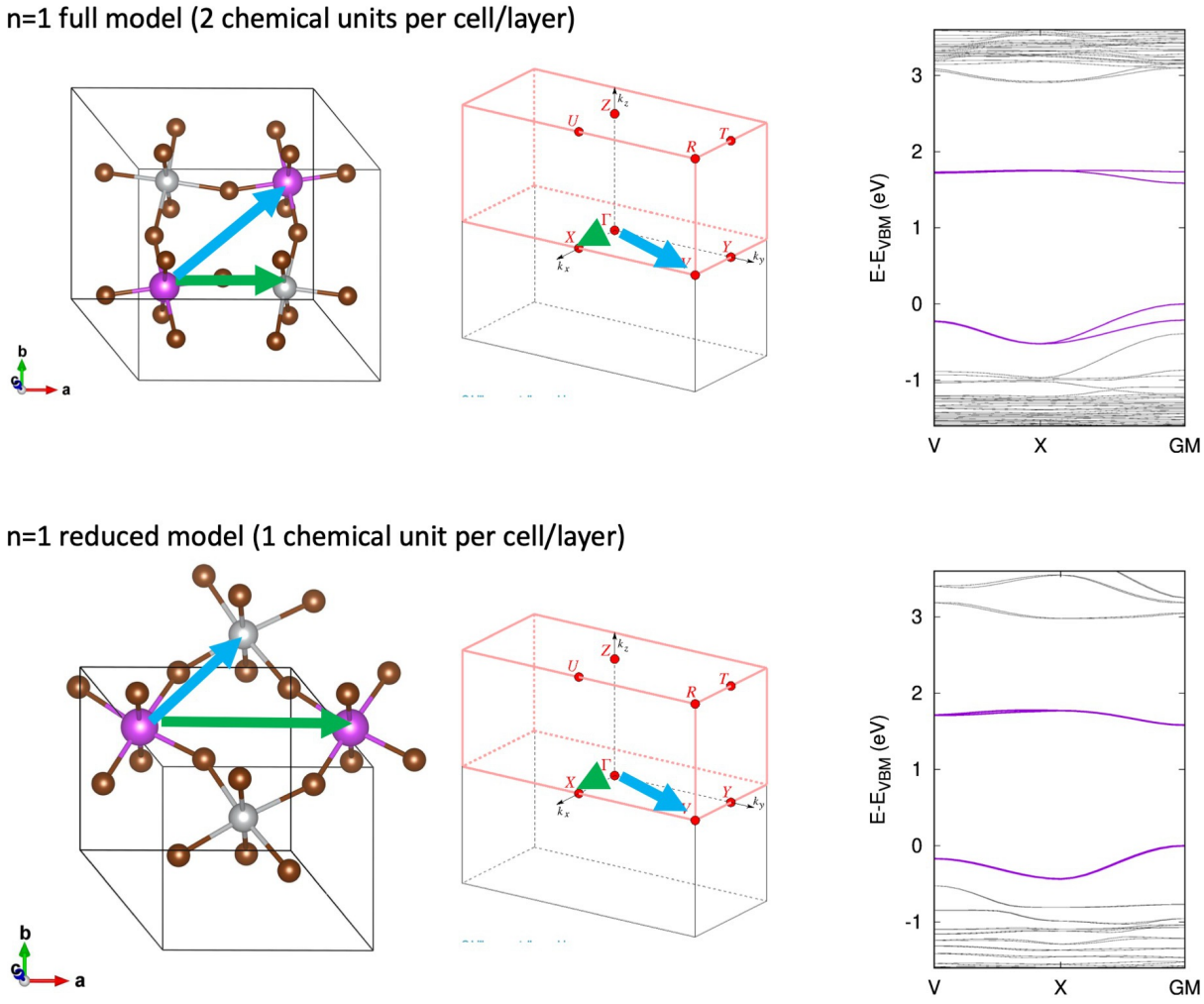

Figure S4. Full and reduced model for n=1 layered double perovskite PeABr1. Corresponding Brillouin zones and high symmetry directions, as well as single particle band structures are reported. Band folding clearly evident when comparing the dispersion X→Gamma in the two models.

Computed optical absorption on-set as function of the theoretical method adopted

Table S1. Single particle band gaps and exciton resonances as computed from DFT and from the ab-initio solution of the Bethe-Salpeter Equation (BSE). DFT computed single particle band gaps are obtained adopting both PBE and PBE0 exchange-correlation functionals (both including Spin-Orbit-Coupling, SOC). Experimental data are reported as reference.

	code	**3D**	**N=2**	**N=1**
Band-to-band transitions (no excitons)				
PBE+SOC	Espresso	1.87	2.06	1.58
PBE0+SOC	VASP	3.17	3.36	3.02
excitons				
BSE @PBE+SOC	VASP	2.93	3.08	2.87
Experimental reference (Figure 3a of main text)				
UV-vis		2.83	2.97	3.04

Tauc-plot and Elliot fit for the estimate of the exciton binding energies of the investigated 3D and layered double perovskites

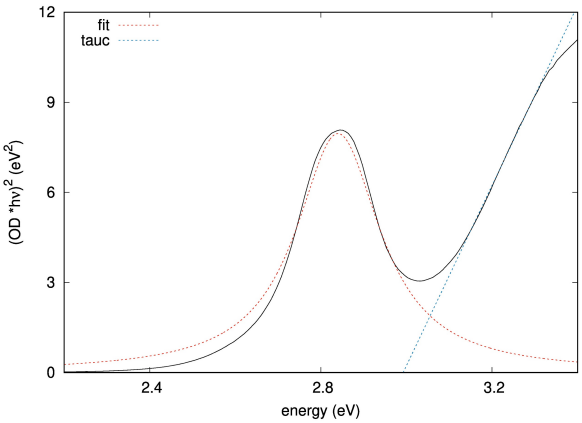

Figure S5. Tauc plot and Lorentzian fitting of the absorption spectrum of 3D $Cs_2AgBiBr_6$ perovskite, for the estimate of the energy of the direct band gap (3.00 eV) and of the exciton binding energy (150 meV).

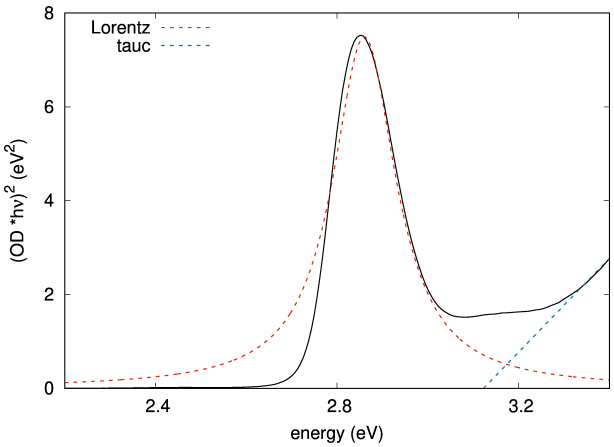

Figure S6. Tauc plot and Lorentzian fitting of the absorption spectrum of layered *n*=2 PeABr2 double perovskite, for the estimate of the energy of the direct band gap (3.12 eV) and of the exciton binding energy (150 meV).

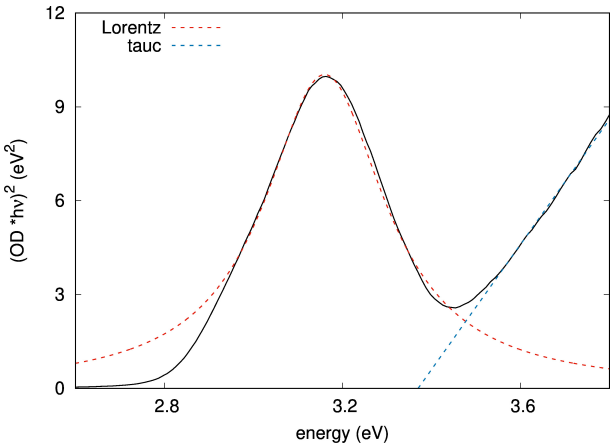

Figure S7. Tauc plot and Lorentzian fitting of the absorption spectrum of layered *n*=1 PeABr1 double perovskite, for the estimate of the energy of the direct band gap (3.35 eV) and of the exciton binding energy (270 meV).

List of BSE calculated excited states

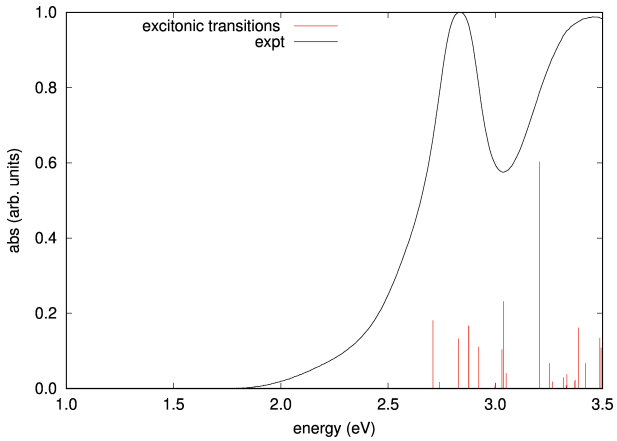

Figure S8. Comparison of the experimental absorption spectrum of $Cs_2AgBiBr_6$ with the excitonic resonances computed from our DFT(+SOC)/BSE calculations. To account for the well-known underestimation of the single particle band gap by standard DFT simulations, we corrected the spectrum adopting scissor operator.

Potential energy surfaces (PES) in neglecting and including exciton effects

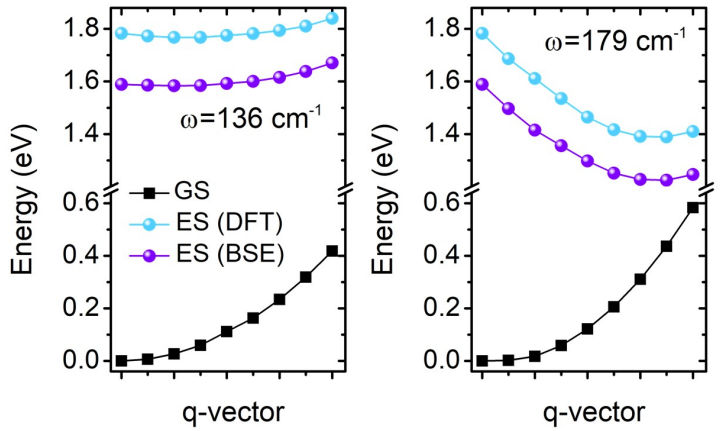

Figure S9. PES calculated for the ground state (GS) and lowest energy excited state (ES) of $Cs_2AgBiBr_6$, probed by distorting the crystal structure along the normal mode with frequency 136 cm^{-1} (left panel) and at 179 cm^{-1} (right panel). ES surface is computed both neglecting exciton effects by considering single particle direct band gap from Density Functional Theory (DFT) and including exciton effects via ab-initio solution of the Bethe Salpter Equations (BSE). Computational details are reported in the main text.

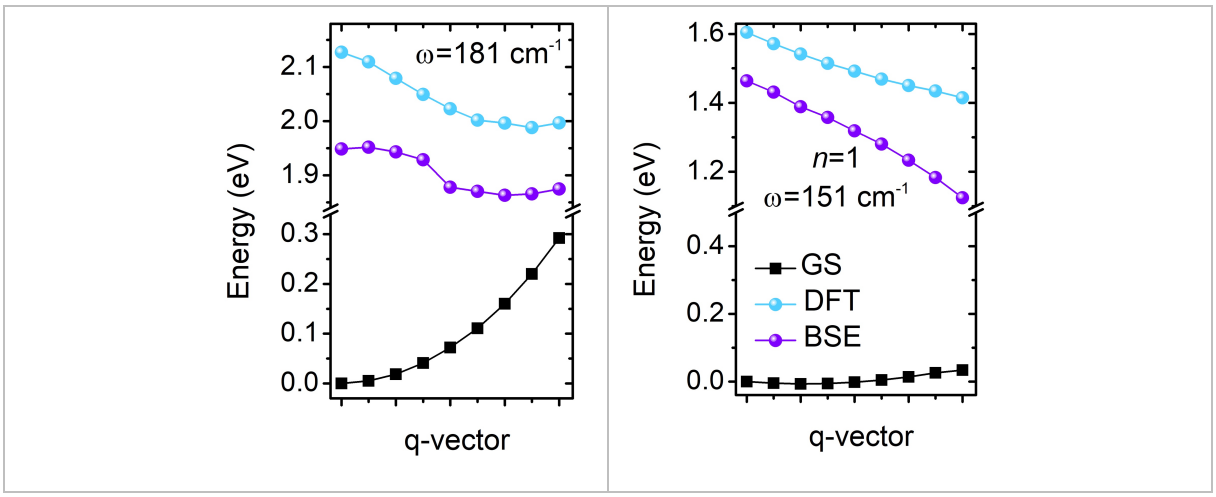

Figure S10. PES calculated for the ground state (GS) and lowest energy excited state (ES) of PeABr2 along the normal mode with frequency 179 cm^{-1} (left panel) and of PeABr1 along the mode with frequency 151 cm^{-1} (right panel). ES potentials both in absence (DFT) and including of exciton effects (BSE) are calculated on model structures with the organic spacer substituted with Cs atoms, as needed to make ab-initio solution of the BSE calculations affordable.

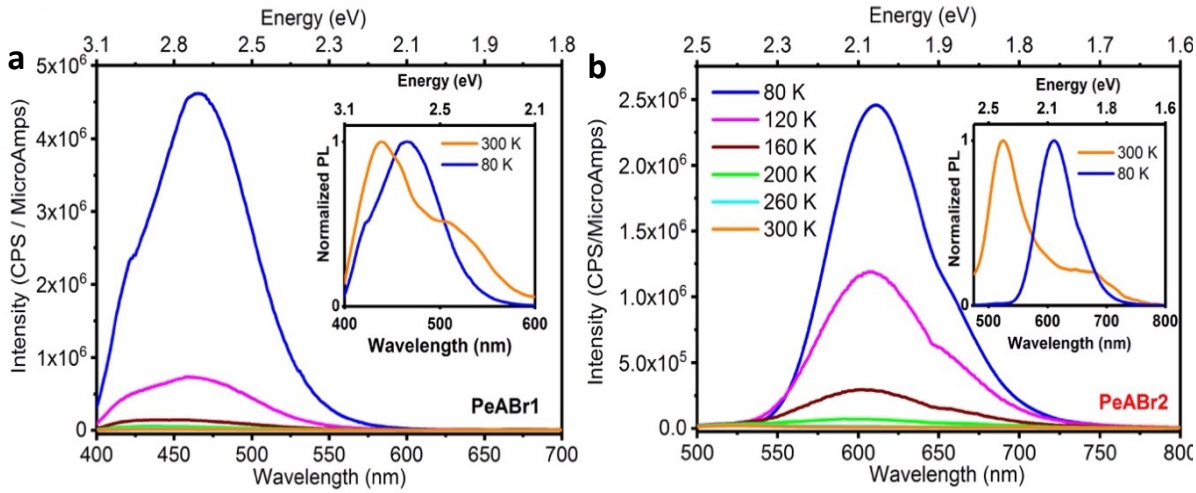

Figure S11. Intensity Dependent PL Spectra for PEABr1 (a) and PEABr2 (b)

Figure above shows the PL spectra upon reducing T. For n=1 a clear emission is observed, despite weak, which however, in contrast with previous literature gains intensity with reducing T. On the other side, the PL for n=2 is completely different. Lowering T, it experiences a severe red shift and it increases in intensity, showing a broad below gap emission. Measuring the PLQY it reveals a 10 fold increase with respect to n=1. In the inset of the figure, the red shift of 2.86 eV to 2.66 eV when decreasing a temperature can be observed. Such band can be assigned to mid gap states, as a result of possible self-trapping. We believe that the initial blue-shift, as observed by the referee, is not real, but it falls within the experimental spectral resolution.

List of computed vibrational frequencies and relaxation energies ΔE

Table S3. Relaxation energies associated to layered and 3D double halide perovskites, calculated for low frequency (<210 cm^{-1}) normal modes.

PeABr1			**PeABr2**			**$Cs_2AgBiBr_6$**	
freq (cm-1)	ΔE (meV)		freq (cm-1)	ΔE (meV)		freq (cm-1)	ΔE (meV)
0.0	0.0		-22.0	9.5		-22.3	0.0
0.0	0.0		-19.8	2.9		-22.3	0.0
0.0	0.0		-4.5	0.0		-22,3	0.0
9.7	0.0		-29	0.0		0.0	0.0
17.4	0.0		-2.0	0.0		-0.0	0.0
23.1	0.0		3,1	13.3		-0.0	0.0
23.3	0.0		15.4	4.7		32.5	0.0
26.2	0.0		17.2	0.0		32.5	0.0
27.8	0.0		21.3	0.0		32.5	0.0
30.1	0.0		21.8	0.3		33.7	0.0
30.6	0.0		23.8	0.0		33.7	0.0
31.3	0.0		24.8	0.0		33.7	0.0
32.9	0.0		28.9	0.0		36.9	0.0
33.3	0.0		29.9	0.0		36.9	0.0
35.1	0.0		30.9	0.0		36.9	0.0
37.0	0.0		36.5	0.0		47.7	0.0
37.1	0.0		37.3	0.0		47.7	0.0
37.3	0.0		38.6	0.0		47.7	0.0
38.6	2.0		41.3	0.0		66.5	0.0
40.7	0.0		41.7	0.0		66.5	0.0
41.4	0.0		42.5	0.0		66.5	0.0
42.1	0.0		43.1	0.0		99.0	0.0
43.1	0.0		45.7	0.0		99.0	0.0
44.7	0.0		46.5	0.0		99.0	0.0
4.1	0.0		47.8	0.7		135.9	80.8
46.8	0.0		48.0	0.8		135.9	84.2
47.3	0.0		48.5	0.0		145.5	0.0
47.8	0.0		50,5	0.0		145.5	0.0
48.2	0.0		51.9	0.0		145.5	0.0
50.0	1.4		52.6	0.0		178.9	629.5
50.8	0.0		53.2	1.3			
51.1	0.0		53.4	0.0			
51.6	0.0		54.5	2.0			
52.0	0.0		55.7	0.0			
52.7	0.0		57.3	0.0			
53.2	1.7		58.0	4.8			
54.1	0.0		59.0	2.3			
54.6	0.0		59.6	1.2			
55.0	0.0		60.8	0.0			

56.3	0.0		62.2	0.0			
57.3	0.0		62.8	0.0			
57.9	0.0		64.5	0.0			
59.3	0.0		65.2	0.0			
60.0	1.6		66.1	0.0			
60.9	1.8		68.9	0.0			
61.4	0.0		69.0	0.0			
61.7	0.9		70.5	0.0			
61.8	0.0		72.1	0.0			
63.4	0.0		75.2	0.0			
64.5	0.0		75.6	0.0			
64.6	0.0		76.2	0.0			
65.3	0.0		77.7	0.0			
65.4	0.0		79.0	8.1			
65.5	0.0		82.4	0.0			
65.9	0.0		84.2	0.0			
66.4	0.0		87.4	9.0			
68.1	0.0		88.5	4.5			
68.8	0.0		89.2	0.0			
70.8	0.0		90.8	0.0			
71.1	0.0		92.5	0.0			
71.8	0.0		92.9	0.0			
72.7	0.0		94.3	0.0			
73.9	0.0		98.7	0.0			
74.1	0.0		101.3	0.0			
74.3	0.0		105.9	0.0			
75.1	0.0		108.4	0.0			
75.8	0.0		111.0	0.0			
76.7	0.0		112.9	0.0			
77.9	0.0		113.2	0.0			
78.7	0.0		115.0	0.0			
79.6	0.0		117.7	0.0			
80.0	0.0		118.6	0.0			
81.7	0.0		130.7	0.0			
82.3	0.0		131.9	0.0			
82.9	0.0		133.1	0.0			
85.1	0.0		134.3	0.0			
87.8	0.0		137.3	0.0			
88.5	0.0		138.8	0.0			
88.8	0.0		142.6	0.0			
89.6	0.0		144.6	0.0			
90.9	0.0		145.5	0.0			
93.0	8.0		147.1	0.0			
95.0	0.0		151.7	0.0			
97.1	0.0		152.8	0.0			
99.2	0.0		154.2	0.0			
100.4	6.5		159.2	0.0			
103.2	0.0		160.9	0.0			

103.3	0.0		162.7	0.0			
106.1	0.0		165.5	0.0			
107.6	0.0		167.3	0.0			
109.4	0.0		179.7	0.0			
110.3	0.0		180.7	221.2			
114.2	0.0		183.9	66.0			
115.4	0.0		185.7	24.2			
115.8	0.0		20.8	0.0			
116.4	0.0		207.2	0.0			
117.3	0.0						
121.6	0.0						
124.9	0.0						
125.6	0.0						
125.8	0.0						
127.5	0.0						
128.7	0.0						
130.6	0.0						
134.7	0.0						
136.5	0.0						
138.4	0.0						
142.3	0.0						
142.8	0.0						
144.0	0.0						
144.1	0.0						
149.0	63.1						
151.2	168.3						
152.9	87.5						
153.5	0.0						
154.0	0.0						
158.9	0.0						
160.4	0.0						
163.6	0.0						
164.6	0.0						
166.0	0.0						
170.2	0.0						
171.0	0.0						
173.0	0.0						
187.4	0.0						
199.8	0.0						
207.2	0.0						
208.5	0.0						